Andrew J. Skinner and Martin F. Lambert
Evaluation of a warm-thermistor flow sensor for use in automatic seepage meters
IEEE Sensors Journal, 2009; 9(9):1058-1067

DOI: 10.1109/JSEN.2009.2024056

Evaluation of a warm-thermistor flow sensor for use in automatic seepage meters

by

Skinner, A.J., and Lambert, M.F.

IEEE Sensors Journal

Citation:
Skinner, A.J., and Lambert, M.F. (2009). ”Evaluation of a warm-thermistor flow sensor for use in automatic seepage meters”. IEEE Sensors Journal, Vol. 9 , No. 9, September, 1058-1067.

For further information about this paper please email Martin Lambert at Martin.Lambert@adelaide.edu.au

Evaluation of a warm-thermistor flow sensor for use in automatic seepage meters

Andrew J. Skinner FIEAust, Martin F. Lambert FIEAust

***Abstract*—**A warm thermistor flow sensor is evaluated for use in an automatic seepage meter measuring very slow groundwater inflows into open water bodies. A novel control circuit allows a single self-referencing thermistor to operate with a constant heat output of 36.8mW while monitoring the thermistor's internal temperature T_S and T_F under still-water and flow conditions respectively. The resultant temperature difference T_S-T_F is the output signal from the instrument. This device is particularly sensitive to very slow fluid flows in the range 0.03 mm/s to 3 mm/s where buoyancy problems have traditionally prevented the use of warm thermistor flow meters. For flow speeds below 3 mm/s the sensor response was shown in the laboratory to be nearly linear with no offset term. Two flow-calibration set-ups were investigated; a precision plunging-probe apparatus and a single-step flow calibration system based upon a Hagen-Poiseuille flow regulator and a vertical standpipe. A numerical (CFD) model of the spherical thermistor agreed well with the two experimental calibration procedures over the flow range between 0 and 3 mm/s. The theoretical model – based on the Peclet number – fits the CFD model well between 3 mm/s and 100 mm/s, but does not hold true in the buoyancy range below 3 mm/s. For a seepage meter funnel having a bell-to-throat area ratio of 2964, groundwater flow velocities as low as 0.01 µm/s (0.9 mm/day) could be measured using this sensor.

***Index Terms*—Slow flow, warm thermistor flow meter, buoyancy, seepage meter.**

I. Introduction

Many of the flow metering techniques used in industrial applications (Spitzer 2005) have finite limits at slow fluid velocities in the order of 10 mm/s. By comparison, many environmental flow rates occur two or more orders of magnitude below this, examples being the rate of sap flow in plants, the percolation rate of rainfall through the landscape, flows in the benthic boundary layer of lakes, the movement of water through sandy river banks or in the swash zone of beaches, or the seepage rate of groundwater into river beds. Of these various applications, the slowest free-water flows are measured by seepage meters; drum- or bell-shaped devices inserted into the sediment of rivers and lakes and used to accelerate groundwater inflows into the range of fluid velocities measurable by conventional flow meters. Taniguchi and Fukuo (1993) used a heat-pulse flow meter fitted to a 500 mm diameter collection funnel having a bell-to-throat area ratio of 2066:1 to measure specific seepage rates from 0.2 µm/s to 5 µm/s, corresponding to sensor flow velocities in the range 0.41 mm/s to 10.3 mm/s. Paulsen et al. (2001) used a transit-time ultrasonic flow meter to resolve specific groundwater discharges of 0.25 µm/s to 25 µm/s using a bell-to-throat area ratio of 2964:1. The Paulsen ultrasonic flow meter was able to measure throat flow velocities in the range from 0.7 mm/s to 74 mm/s. Rosenberry and Morin (2004) used commercial electromagnetic flow meters to investigate the temporal variability of lake seepage. These researchers used galvanised tanks covering 17,670 cm^2, which is 6.9 times larger than the conventional ½ x 200-litre drum first introduced by Lee (1977), and giving them a bell-to-throat ratio of 3487:1. Nevertheless, their minimum detectable flow velocity was 0.65µm/s (56 mm/day) because of the inherent limitation of the sensor's own minimum flow rate of 2.2 mm/s.

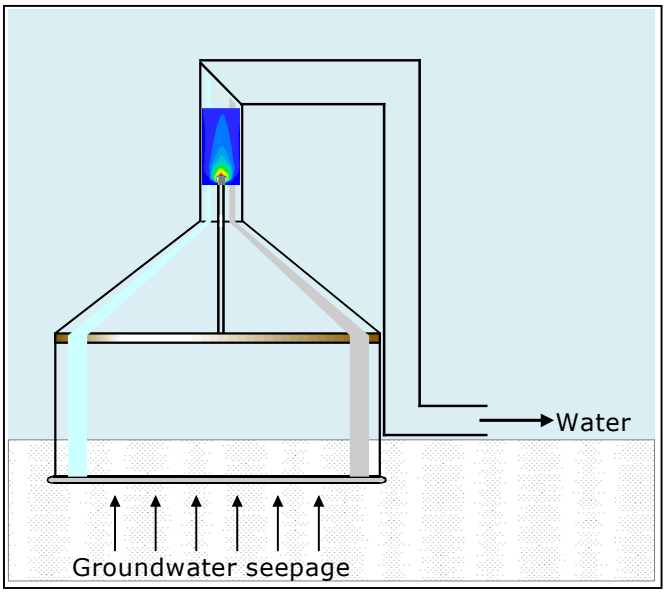

Figure 1 Schematic diagram of an automatic seepage meter (after Taniguchi and Fukuo 1993) adapted to use a warm thermistor flow meter rather than a heat pulse sensor

Manuscript received March 2008. This work was supported by Measurement Engineering Australia of Adelaide South Australia as part of an industrial PhD program in association with the Department of Civil and Environmental Engineering at Adelaide University

A. J. Skinner is the Engineering Director at Measurement Engineering Australia Adelaide South Australia phone: 618 8332 9044; fax: 618 8332 9577; (e-mail: andrew.skinner@mea.com.au).

M. F. Lambert is an Associate Professor at the School of Civil and Environmental Engineering at Adelaide University, Adelaide, South Australia 5005 (e-mail: mlambert@civeng.adelaide.edu.au).

Seepage meters are an application where the vertical flows in the throat of the funnel are in the same direction as buoyancy-induced flows from a thermal flow sensor (Figure 1). These very same buoyancy-induced errors have limited the lowest warm-thermistor velocity measurements in lakes to flows above 3 mm/s (eg. MacIntyre 1986). If warm thermistor slow-flow metering technology can be made to work in the sub-3 mm/s range, it could also be adapted for horizontal flow measurements in porous materials such as beach sands (e.g. Riedl and Machan 1972).

While warm-thermistor flow meters have been used for over thirty years, efforts to upgrade such sensors using modern electronic circuit techniques seem worthwhile, given their inherent simplicity and low cost in comparison to other slow-flow measurement techniques such as particle image velocimetry (Roy et al., 2002) or gas diffusion sensors (Brand et al., 2007).

A. *A Theoretical Model of a Spherical Flow Sensor*

What then is the theoretically 'slowest detectable' flow rate of a spherical warm thermistor flow sensor in water? Clift et al (1978) related the heat loss from a spherical heat source to the dimensionless Peclet number ***Pe***, which is the ratio of advective heat loss to the rate of thermal diffusion. In the case of thermal diffusion, the Peclet number ***Pe*** is the product of the Reynolds number ***Re*** and the Prandtl number ***Pr***.

The heat flux $\boldsymbol{Q}$ (W/m^2) from a sphere in a flow stream is: -

$$Q_{flow} = \frac{k\Delta T_F}{d}(1+(1+P_e)^{1/3}) \quad (1)$$

within 2% over the flow range of ***Pe***, where ***k*** is the thermal conductivity of water (0.58 W.m^{-1}.K^{-1} at 25°C), $\boldsymbol{\Delta T_F}$ is the temperature difference $\boldsymbol{T_F}$-$\boldsymbol{T_A}$ under fluid flow conditions between the surface temperature $\boldsymbol{T_F}$ of the sphere and the ambient temperature $\boldsymbol{T_A}$ of the fluid a long way from the sphere, ***d*** is the diameter of the sphere and ***Pe*** is the Peclet number, which is defined as: -

$$P_e = \frac{vd}{\alpha} \quad (2)$$

where $\boldsymbol{\alpha}$ is the thermal diffusivity of the surrounding medium and $\boldsymbol{v}$ is the velocity of the creeping (laminar) flow.

In the absence of flow (under still water conditions) the heat loss is

$$Q_{still} = 2\frac{k\Delta T_S}{d} \quad (3)$$

where $\boldsymbol{\Delta T_S}$ is the temperature difference $\boldsymbol{T_S}$-$\boldsymbol{T_A}$ under no-flow (still water) conditions between the surface temperature of the sphere $\boldsymbol{T_S}$ and the ambient temperature $\boldsymbol{T_A}$ of the fluid a long way from the sphere.

Equations 1 and 3 can be combined to express the temperature difference $\boldsymbol{T_S}$-$\boldsymbol{T_A}$-$\boldsymbol{T_F}$+$\boldsymbol{T_A}$= $\boldsymbol{T_S}$-$\boldsymbol{T_F}$ between flow and still-water conditions, while eliminating the need to make an extra measurement of ambient temperature ($\boldsymbol{T_A}$) via a second thermistor.

$$T_S - T_F = \frac{Q\cdot d}{k}\left(\frac{1}{2} - \frac{1}{\left(1+\left(1+\frac{v\cdot d}{\alpha}\right)^{\frac{1}{3}}\right)}\right) \quad (4)$$

Equation 4 suggests that a spherical warm thermistor sensor, operating with a constant heat flux $\boldsymbol{Q}$ (W/m^2) and capable of detecting its own operating temperature under flow and no-flow conditions should be able to monitor flows down to 0 mm/s. Flow resolution will be dependent only on the instrument's ability to resolve temperature differences between still water and flow conditions.

Bio-film build up on a thermistor sensor in the throat of a seepage meter funnel is a source of calibration drift during long-term deployment in a biologically active natural water body. The sensitivity of the temperature difference $\boldsymbol{T_S}$-$\boldsymbol{T_F}$ to the spherical diameter of the thermistor sensor is shown in Figure 2. This in turn suggests that a working instrument needs to prevent this bio-film build up by the conventional means of regular biocide injections into the measurement chamber or by irradiating the thermistor surface with ultraviolet light at the germicidal wavelength of 254.7nm.

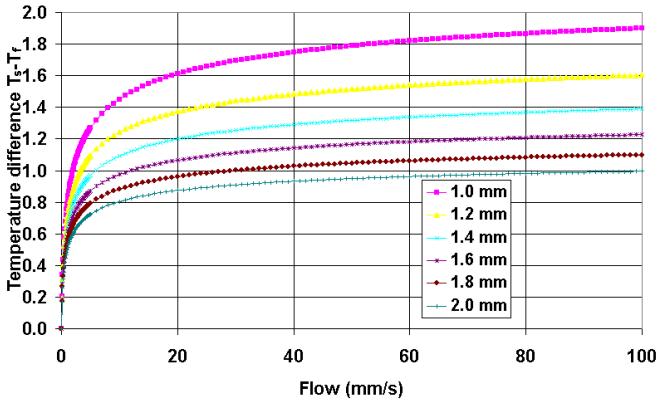

Figure 2 The theoretical temperature difference $\boldsymbol{T_s}$-$\boldsymbol{T_f}$ versus flow rate over the range 0 to 100 mm/s is described by Equation 4. It can be seen to be particularly sensitive to the diameter of the thermistor's spherical bead, which is in turn sensitive to build-up of a bacterial biofilm on the device under natural field conditions.

B. *Numerical Methods for Sensor Modelling*

Computational fluid dynamics (CFD) – based on numerical solutions to the Navier-Stokes Equations – provides a useful tool for visualising and modelling just what happens to a constant-power thermistor operating in the flow range below 3 mm/s being tested experimentally in this paper. In addition, it provides a response curve for the sensor over the extended flow range between 0 mm/s and 100 mm/s. The model tested was that of a horizontal probe with upward flow in the direction of buoyant plume flow, as would be found in a seepage meter throat having a side-mounted sensor package.

The thermistor was modelled as a 1.0 mm cubic heat source inside a 0.1 mm thick glass 'skin' on the end of a 12 mm glass rod, and dissipating a nominal 40mW of heat into the fluid (Figure 4).

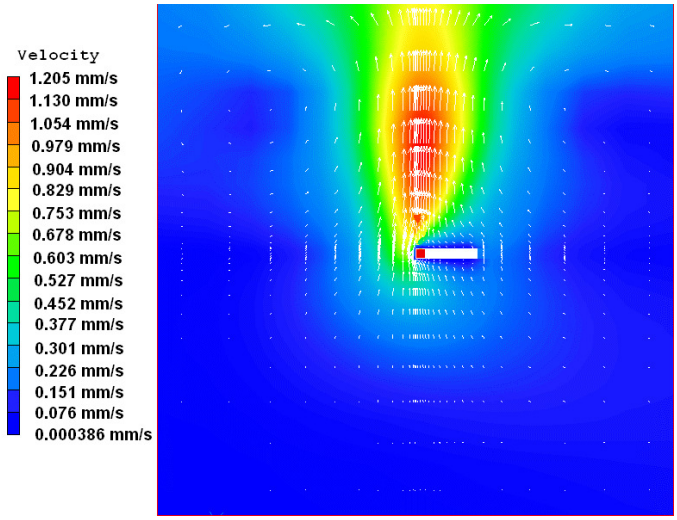

Figure 3 A CFD model of the velocity profile within the buoyant plume rising above the tip of a horizontal glass-rod thermistor under no-flow conditions. Note that the upward flow velocities generated by the buoyant plume are as high as 1.2 mm/s at about 25 mm above the warm thermistor tip. The model domain is 100 mm x 100 mm, and one can see (in the white streamlines) that circulating currents were beginning to form when the CFD model was stopped.

The CFD model was run for flow rates over the range 0 mm/s to 100 mm/s, with the temperature of the heater element being recorded as the output from the model. Each temperature was used to derive a temperature difference T_S-T_F, where T_S is the still-water probe temperature at 0 mm/s with the sensor generating the maximum buoyant plume and T_F is the temperature of the probe under flow conditions.

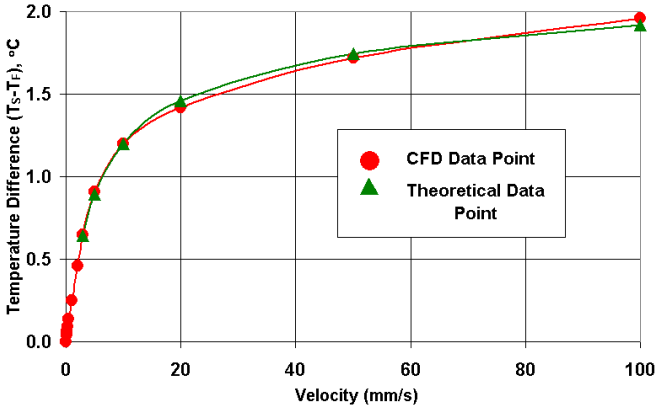

Figure 4. CFD model response: The temperature difference T_S-T_F between the sensor temperature T_S under still water conditions and the sensor temperature T_F under flow conditions is shown for flow rates between 0 and 100 mm/s. Note the near-linear response at velocities below about 3 mm/s; this is shown more clearly in later figures. The theoretical model based on the Peclet number is shown for comparison (green triangles) and can be seen to provide a reasonable approximation to the CFD data for flows above 3 mm/s once linear scaling factors (offset and gain) have been applied.

Figure 4 shows the response of the model over the flow range 0 mm/s to 100 mm/s. Between 0 and 3 mm/s, buoyant advection dominates flow-induced advection, and the response is almost linear. In the extended flow range between 3 mm/s and 100 mm/s, flow-induced advection dominates buoyant advection and is well characterised by the theoretical Peclet number model of Equation 4.

II. A CONSTANT POWER THERMISTOR FLOW METER

A. *Choosing a thermistor*

The thermistor chosen for this sensor is a hermetically-sealed Honeywell 120-102EAJ-Q01 mini glass probe thermistor (Figure 5) whose long glass shaft allows the sensing tip to be located about ten diameters away from the more thermally conductive stainless-steel metal shaft that supports the sensor. The thermistor has an electrical resistance R_T of 1kΩ ±20% at 25ºC and a negative temperature coefficient. A low-resistance thermistor was chosen to ensure that V^2/R_T heat loss is as high as practicable given the limited drive voltage available in a 12V battery-powered field measurement system.

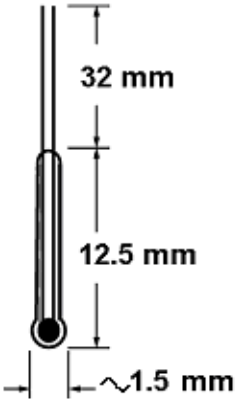

Figure 5. Honeywell 121-102EAJ-Q01 mini Glass Probe thermistor used to measure both ambient temperature and fluid flow.

The thermistor is driven into self-heating mode by a voltage V_T, such that the power output P_T is 36.8 mW. At warmer water temperatures and lower thermistor resistances, current increases, voltage decreases, but the power dissipated by the thermistor is held constant by the sensor control circuitry.

The 'thermal dissipation constant' of a thermistor is defined by thermistor manufacturers to be the power in milliwatts required to raise the thermistor's internal temperature by 1°C in a specified fluid at a specified flow rate. The dissipation constant for the mini glass rod thermistor of Figure 5 was measured at 0.8 mW/ºC in still air, 4.1 mW/ºC in still water and 6.1 mW/°C in a strong jet of water. At high flows there is no rise in the water temperature at the surface of the thermistor, as all the heat is transported away, making the device insensitive to minor flow variations. The temperature rise in this sensor while dissipating 36.8 mW of power was measured at 9.0ºC above ambient in still water and 6.0ºC above ambient in a strong water jet. The working range of the

sensor between zero flow and maximum measurable flow is therefore only 3.0ºC, which sets a requirement for high precision of temperature measurement to obtain adequate instrument sensitivity.

B. *Constant power control circuitry*

The constant-power warm-thermistor control circuit (Figure 6) used to monitor the self-heated thermistor in this application has been described by Skinner and Lambert (2008). This analog control circuit has infinite precision and a wide dynamic range, making it suitable for a transducer capable of operating over three orders of magnitude of flow and three orders of magnitude of output power.

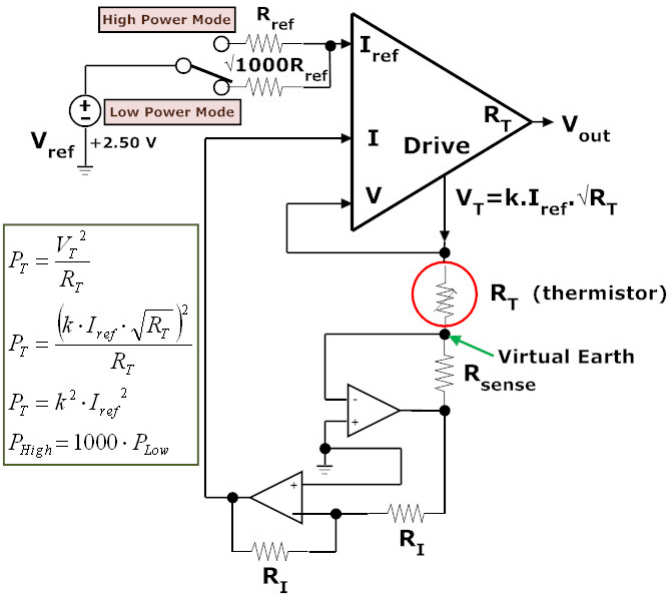

Figure 6 The 'double-bridge' control circuit of Skinner and Lambert (2008) forces constant power dissipation from a thermistor operating in either zero-heating (low power) or self-heating (high power) mode while providing a separate output proportional to the thermistor's resistance. Sensor calibration allows this resistance to be reported as a temperature. The 'mode switch' allows the device to be switched over a power range of 1:1000

The thermistor resistance $\boldsymbol{R_T}$ is measured and transmitted as a voltage $\boldsymbol{V_{out}}$ while self-heating is occurring. The thermistor's temperature $\boldsymbol{T}$ is derived from this resistance $\boldsymbol{R_T}$ via the Steinhart-Hart equation (Steinhart and Hart 1968) and sensor specific calibration coefficients $\boldsymbol{a}$, $\boldsymbol{b}$ and $\boldsymbol{c}$: -

$$T(°C) = \frac{1}{a + b\ln(R) + c\ln(R)^3} - 273.15 \qquad (5)$$

At the same time, the thermistor is self-heated by the control circuit's output voltage $\boldsymbol{V_T}$, which is forced to be equal to the product of the reference current $\boldsymbol{I_{ref}}$ and the square root of thermistor resistance $\boldsymbol{R_T}$, such that power dissipated in the thermistor is proportional to $\boldsymbol{V_T^2/R_T}$, or $\boldsymbol{(I_{ref}\sqrt{R_T})^2/R_T}$, which is constant and dependent only upon $\boldsymbol{I_{ref}^2}$.

III. Calibration Method #1

Two different sensor calibration methods were trialed. The first of these is a laboratory method to determine the sensor response in the 0.1 mm/s to 3 mm/s range where the CFD model indicated that the temperature difference $\boldsymbol{T_S}$-$\boldsymbol{T_F}$ would be nearly linear, and where buoyancy-induced flow plays a large part in determining the sensor response. Calibration Method #1 is a linear motion generator that drives the probe vertically downward through a very still isothermal water body under precisely controlled conditions. Calibration Method #2 (Section IV) – still in the laboratory – sought to more closely simulate the conditions that the sensor would face inside the vertical throat of a bell-shaped seepage meter (Figure 1). Here water flows upward past a stationary sensor element and at flow rates roughly encompassing the range obtainable with Calibration Method #1. This second method provides a more general – and quicker – solution to sensor calibration.

A. *A precision 'plunging-probe' method for testing buoyancy effects*

In Calibration Method #1 (Figure 7), a single glass probe thermistor was mounted on a 250 mm long length of stainless-steel tube having an outside diameter of 2.5 mm. This sensor was inserted into a 20-litre Dewer vessel containing well-mixed water that had been allowed to come to rest at a near-constant temperature. The test tank was capped with a 50-mm cork insulated lid with a small access hole for the probe that limited heat gain or loss from the tank so that background ambient temperature changes were as small as practicable during the measurement sequence.

Measurement of the resistance output voltage $\boldsymbol{V_{out}}$ of the sensor controller circuit shown in Figure 6 was made with a Keithley K2000 6½-digit precision voltmeter capable of resolving 0.001°C. Resistance-to-voltage calibration of the control circuit was carried out using a series of precision resistors in place of the thermistor, achieving a linear calibration ($\boldsymbol{r^2}$=1.00) over the expected operating resistance range of the instrument. The thermistor resistance was converted to temperature via the Steinhart-Hart Equation using calibration coefficients determined for this specific 1kΩ@25°C thermistor against a Hart 1506 precision thermometer in a well-stirred calibration bath.

B. *Precision flow sensor drive*

The generation of precise flow velocities down to 0.1 mm/s was achieved using a single DC-Micromotor (Faulhaber 2224R012S) coupled to a range of precision all-metal spur gear heads (Faulhaber 22/2) as shown in Figure 7.

This motor-gearbox was directly coupled to a precision shaft-encoder (Unidata 6509) driving a beaded cable to provide a non-slip linkage to the probe on one-side and a counterweight on the other. This assembly allowed the sensor to be moved vertically through a very still water column in the aforementioned 20 litre Dewar vessel. The linear velocity $\boldsymbol{\nu}$ of the sensor, in mm/s, was calculated as $\boldsymbol{\nu = l/t}$ from the known

distance l in millimetres travelled by the probe (read off the shaft encoder's LCD display) in a time period t measured with a stopwatch.

A control circuit was built to drive the probe up and down through the water column at various speeds (achieved by using different motor drive voltages for each gearbox ratio). The thermistor resistance was measured while the probe was operating in various ambient, self-heated, stopped, forward and reverse modes. These operating sequences are shown in Table 1. The temperature difference T_S-T_F between stages 3 and 4 ('rising flow') and 7 and 8 ('reverse flow') was used to determine the sensor's response at each flow speed. Voltage measurements were synchronised with each operating condition, and recorded within the K2000 meter's internal memory under computer control.

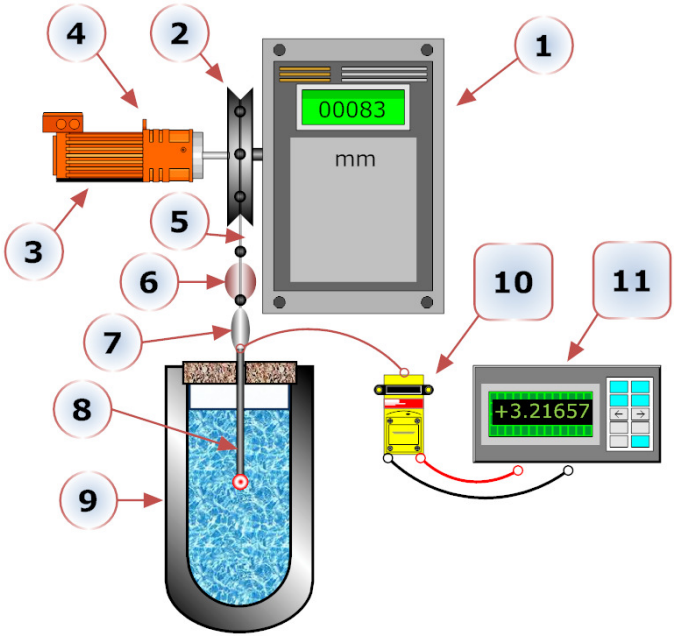

Figure 7 'Plunging-probe' sensor calibration rig for generating very slow linear velocities for a warm-thermistor probe in an isothermal still water tank. A shaft-encoder [1] having a pulley wheel [2] of 500mm circumference, precision bearings and 1 mm resolution is driven by a DC-Micromotor [3] coupled to a precision all-metal spur gear head [4]. A beaded line [5] is balanced across this pulley wheel by lead counterweight [6] and the lead weight [7] on the stainless-steel shaft [8] carrying the thermistor. The motor raises and lowers the probe through the very still temperature-stable water body in the 20-litre Dewar vessel [9]. The output of the constant-power bridge circuit [10] is recorded by the 6½-digit Keithley K2000 recording multimeter [11]. Power supply and control circuits are not shown.

TABLE 1 MEASUREMENTS OF PROBE TEMPERATURE WERE MADE UNDER EIGHT DIFFERENT CONDITIONS FOR EACH OF THE 23 SIMULATED FLOW SPEEDS. THIS CALIBRATION REGIME ENSURED THAT ALL POSSIBLE COMBINATIONS OF FLOW CONDITIONS OCCURRED FOR EACH FLOW VELOCITY.

Stage #	Ambient/Heated	Stopped/ Moving	Dir'n
1	Ambient	Stopped	-
2	Ambient	Moving	Down
3	Heating	Moving	Down
4	Heating	Stopped	-
5	Ambient	Stopped	-
6	Ambient	Moving	Up
7	Heating	Moving	Up
8	Heating	Stopped	-

C. *Flow results using the 'plunging probe' calibration rig*

Twenty-three different flow speeds were generated in the flow range 0.1 mm/s to 3 mm/s using the 'plunging probe' calibration rig #1. Both the experimental and CFD temperature difference T_S-T_F are plotted against velocity in .

At flow velocities v below 3 mm/s the self-heated probe 'flow' temperature T_F approaches the 'still water' self-heated temperature value T_S. The experimental temperature difference T_S-T_F was found to be linearly proportional to flow speed in mm/s with no offset term: -

$$v = 4.44(T_S - T_F) \tag{6}$$

with the proportion of variance explained r^2 = 99.45%

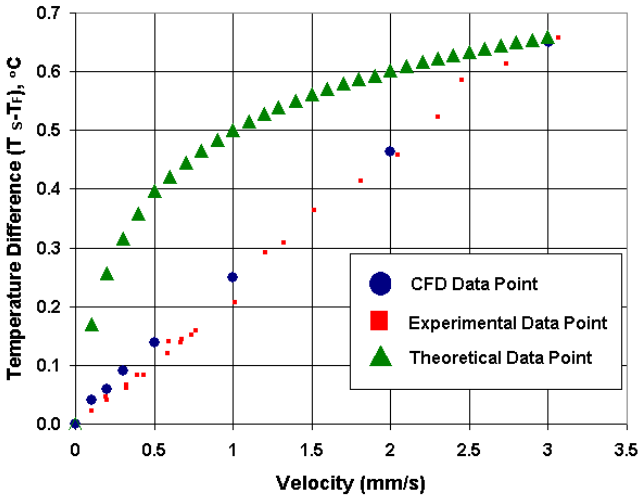

Figure 8. Temperature difference T_S-T_F versus flow speed for a constant-power self-heated flow sensor for calibration rig #1 under rising flow conditions. The large circular data points result from the CFD modelling, while the smaller square data points were recorded using the 'plunging probe' sensor calibration rig. Note that the Peclet Number model of Equation 4 (green triangles) does not represent either the experimental or CFD data in this 'buoyancy range' below 3 mm/s

The CFD modelled data, plotted on the same graph as the experimental results in Figure 8, shows excellent agreement between the two, despite the small discrepancies between the modelled and experimental power outputs (40 mW versus 36.8 mW respectively) and thermistor shapes (cubic versus spherical respectively). Between 0 and 3 mm/s the CFD model is characterised by the linear equation:

$$v = 4.45(T_S - T_F) \tag{7}$$

with an r^2 value of 99.16%.

By contrast, Equation 4 breaks down in this sub-3 mm/s range (Figure 8, green triangles) as it does no incorporate a mechanism to account for the vertical buoyancy-induced flows generated in the surrounding fluid by the sensor itself.

The sensitivity of the analog control circuit is infinite by definition, and so is defined in practice by the DC voltage resolution of the analog-to-digital converter used to monitor the thermistor's temperature during still-water and flow measurements. The 6½-digit Keithley K2000 recording multimeter has a resolution of 10μV on the 10V DC range. The Skinner-Lambert Bridge of Figure 6 has a sensitivity of

400 Ω/V when converting thermistor resistance to output voltage. The Keithley voltmeter is therefore able to resolve temperature differences of approximately 0.001°C (≈0.4mΩ) at the warmest expected water temperature of 35°C where the thermistor ***R-T*** response is least sensitive. As equation 6 can be re-written as

$$\left(T_S - T_F\right)\Big/_{V} = 0.225°C\Big/_{mm \cdot s^{-1}} \quad (8)$$

then the smallest resolvable velocity measurable by the apparatus of Figure 7 is **0.0044 mm/s**.

IV. CALIBRATION METHOD #2

The 'plunging probe' design of Calibration Method #1 has a much higher precision than the flumes, linear tow-tanks and rotating arms over circular ponds described in the literature for calibrating warm-thermistor flow sensors. However, a calibration environment was sought that more closely resembled that found in a vertical seepage meter standpipe, and one which would allow a single-sweep calibration encompassing all flow velocities consecutively. The flow generation process developed is reliant upon first principles and upon measurands - time and depth - that can be measured accurately and with commonly available equipment. The sensor is placed in a vertical pipe environment (Figure 9), just as it would be in the throat of a seepage meter.

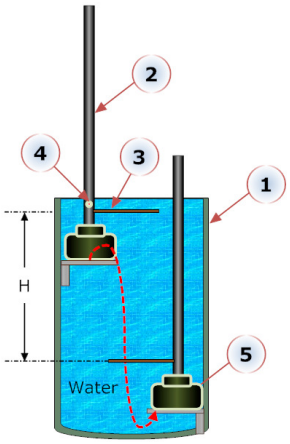

Figure 9. A **'single-sweep' seepage meter calibration system.** This step-change variable head seepage meter calibrator uses a Hagen-Poiseuille flow controller. A 240-litre container [1] holds a 900-mm depth of well-mixed water at room temperature. The thermistor sensor located at level [4] is submerged by 50 mm when the 1000-mm high x 27.5 mm diameter bore vertical calibration sensor standpipe [2] and electronic control circuit [5] are in the top left-hand position. In this initial position, water in the vertical sensor standpipe is at the same level as the surface of the water in the main tank. When the instrument is plunged to the lower right-hand position, a differential head pressure '***H***' is applied to opposite ends of the (coiled) Hagen-Poiseuille flow control pipe [3], which has a 5-mm bore and a length of 33m.

This calibration rig generates a rising flow, and the sensor's thermal heat field and any buoyant circulating currents are subject to the same real boundary conditions present in a field deployment of this type of sensor in a seepage meter. The flow regulator to the sensor stand-pipe is a simple horizontal small-bore pipe which controls the flow rate based only upon the differential pressure head, the dimensions of the pipes and physical properties of the water; these are described by the Hagen-Poiseuille equation.

A. A 'single-sweep' seepage meter calibration system

Between 1839 and 1840, G.H.L. Hagen and J.L.M. Poiseuille studied low-speed flows of fluids having dynamic fluid viscosity μ in circular pipes having fully-developed non-turbulent flows Q with Reynolds numbers below 1000. Flows in such long small-bore pipes are dependent only upon the pressure gradients dp/dx per unit length in a pipe having radius r_0. Based upon publications by Poiseuille in 1840 and 1846, such flows have become known as Hagen-Poiseuille flows; they are an exact solution of the Navier-Stokes equations in fluid mechanics. The relationship between flow, pressure gradient and pipe radius is: -

$$Q_{pipe} = \frac{\pi \cdot r_0^4}{8\mu}\left(-\frac{dp}{dx}\right) \quad (9)$$

where pressure head p is equal to the product of the water density ρ, the gravitational acceleration constant g and the instantaneous water height h.

B. Solving the Hagen-Poiseuille equation for time and water height

The vertical flow-rate in the calibration rig falls as the water height in the sensor standpipe rises; one could solve the time-series equation for either flow or water height. Here the solution for water height is given so that level sensors can be used in determining the system time-constant. The Hagen-Poiseuille equation for flow rate in the small-bore flow-control pipe is first restated: -

$$Q_{pipe} = \frac{\pi \cdot r_0^4}{8\mu}\left(-\frac{dp}{dx}\right)$$

The mean velocity $\bar{u}$ is defined by $\bar{u}=Q_{pipe}/a$ where $a=\pi r_0^2$ and gives: -

$$\bar{u} = \frac{r_0^2}{8\mu}\left(-\frac{dp}{dx}\right) = \frac{1}{2}u_{\max}$$

The pressure gradient dp/dx can be described specifically as the pressure drop $\Delta p/\Delta x$, where $\Delta p=\rho g(H-h)$ and $\Delta x=L$, where L is the length of the flow control pipe between the main tank and the sensor stand pipe. Re-writing the Hagen-Poiseuille equation then gives: -

$$\bar{u} = -\frac{r_0^2 \cdot \rho \cdot g}{8\mu \cdot L}\left(H - h\right)$$

The volume change ΔV per unit time Δt is dependent upon the mean flow-rate and the cross-sectional area of the flow control pipe a, but can also be described by the change in

water height Δh in the sensor stand pipe multiplied by its cross-sectional area A: -

$$\Delta V = a \cdot \bar{u} \cdot \Delta t = A \cdot \Delta h$$

or: -

$$\frac{\Delta h}{\Delta t} = \frac{a}{A} \cdot \bar{u}$$

Substituting for flow-rate: -

$$\frac{\Delta h}{\Delta t} = -\frac{a}{A} \cdot \frac{r_0^{\,2} \cdot \rho \cdot g}{8\mu \cdot L}(H - h)$$

The limit of $\Delta h/\Delta t$ as t approaches 0 is dh/dt. That is: -

$$\frac{dh}{dt} = -\frac{a}{A} \cdot \frac{r_0^{\,2} \cdot \rho \cdot g}{8\mu \cdot L}(H - h) \tag{10}$$

Separating variables: -

$$\frac{1}{(H-h)} \cdot dh = -\frac{a}{A} \cdot \frac{r_0^{\,2} \cdot \rho \cdot g}{8\mu \cdot L} \cdot dt$$

Integrating: -

$$\frac{1}{H} \cdot \ln|H - h| = -\frac{a}{A} \cdot \frac{r_0^{\,2} \cdot \rho \cdot g \cdot t}{8\mu \cdot L} + C$$

$$\ln|H - h| = -\frac{H}{A} \cdot \frac{a \cdot r_0^{\,2}}{\mu \cdot L} \cdot \frac{\rho \cdot g}{8} \cdot t + CH$$

Note the use of the absolute value of $(H-h)$, to prevent the equation describing the log of a negative number.

Evaluating for initial conditions, when $t=0$, $h=0$, $(H-h)=H$: -

$$\ln|H - 0| = 0 + CH$$

$$\therefore C = \frac{1}{H} \cdot \ln H$$

$$\ln(H - h) = -\frac{H}{A} \cdot \frac{a \cdot r_0^{\,2}}{\mu \cdot L} \cdot \frac{\rho \cdot g}{8} \cdot t + \ln H$$

for $H-h > 0$

Taking the inverse log function (exponentiation): -

$$H - h = e^{\left(-\frac{H}{A} \cdot \frac{a \cdot r_0^{\,2}}{\mu \cdot L} \cdot \frac{\rho \cdot g}{8} \cdot t + \ln H\right)}$$

$$h(t) = H - e^{\left(-\frac{H}{A} \cdot \frac{a \cdot r_0^{\,2}}{\mu \cdot L} \cdot \frac{\rho \cdot g}{8} \cdot t + \ln H\right)} \tag{11}$$

This equation can be written in the form: -

$$h(t) = H - e^{\left(\frac{-t}{\tau} + \ln H\right)} \tag{12}$$

where

$$\tau = \frac{A}{a} \cdot \frac{L}{H} \cdot \frac{8}{r_0^{\,2}} \cdot \frac{\mu}{\rho \cdot g} \tag{13}$$

The 'time-constant' τ describes the first-order frequency response of the system, and is the time taken in seconds for the height of the water $h(t)$ in the sensor standpipe to rise to 63.21% of the final height H. This occurs at $t=\tau$ such that

$$h(\tau) = H - e^{\left(\frac{-\tau}{\tau} + \ln H\right)} = H(1 - e^{-1}) \tag{14}$$

Eq. 10 describes the rate of change of height with time, which is the vertical velocity of flow in the standpipe; this must be related to the temperature difference $\Delta T = T_S - T_F$. The maximum flow rate v_{max} (m/s) in the sensor stand pipe occurs at $t=0$ when $h(t)=0$, and is: -

$$v_{\max} = \frac{a}{A} \cdot \frac{r_0^{\,2} \cdot \rho \cdot g}{8\mu \cdot L} H \tag{15}$$

C. Calibration Rig #2 Design

The calibration rig of Figure 9 consists of a horizontal small-bore pipe located below the thermal sensor; the latter is itself co-axially located in the vertical sensor standpipe as it would be in the throat of a seepage meter.

A full range of flows can be obtained between v_{max} and zero using this technique and the flow velocity at any particular moment can be determined from the time elapsed since flow commenced.

A 1m long stainless-steel standpipe having an internal diameter of 27.5 mm was selected. The water inlet to this sensor standpipe is located 170 mm below the thermistor sensor to allow the flow to change direction from horizontal to vertical without creating excessive turbulence at the sensor tip. An additional 50 mm depth of water was allowed for above the sensor so that measurements at maximum velocity (3 mm/s) occurred with the sensor tip well-covered. Early experiments confirmed that Eq. 12 only holds true if flow in the small-bore pipe is truly laminar with a Reynolds Number R_e below 1500, where

$$\mathrm{Re} = \frac{\rho v_s L_C}{\mu} \tag{16}$$

and ρ is the density of the water at ambient temperature T_a, v_s is the mean velocity of water in the small-bore pipe, L_C is the characteristic length (equal to the internal diameter $2r_0$) and μ is the dynamic viscosity of the water.

A small-bore inlet pipe having an internal diameter of 5 mm was therefore chosen to ensure that flow is laminar (Re = 1350) at the maximum standpipe flow rate of 3 mm/s (A/a = 30), giving a maximum flow rate in the inlet control pipe of 90.75 mm/s. This required an inlet pipe length L of approximately 33 m. These dimensions indicate a system time constant of 174 s at a water temperature of 23.6°C and maximum water height H of 780 mm as per Eq. 13.

Because the cross-sectional area of the vertical sensor standpipe is small compared to the cross-sectional area of the main calibration tank (1:425), changes in the pressure head H due to small falls in main tank water level as the empty standpipe fills were ignored. Similarly, small sources of second-order errors were also ignored, such as changes in background water temperature and changes to the radial flow profile in the sensor standpipe as the water level rose.

D. *Testing the system time constant* τ

The theoretical system time constant τ is particularly sensitive to the small-bore radius r_0 and the pipe length L, but also upon the water temperature and the consequent variations in density and dynamic viscosity.

These uncertainties were addressed by measuring the actual time constant before each flow calibration. This was accomplished by inserting 10 x 1kΩ@25°C NTC glass-rod thermistors through the wall of the sensor standpipe to act as active level sensors. These sensors were spaced at heights above the small-bore inlet of 191, 353, 469, 552, 612, 656, 687, 709, 725 and 751 mm. The sensor tip was located 170 mm above the small-bore inlet. These spacings were chosen to give approximately equal time intervals between the arrival of the wetting front at each consecutive level sensor.

All sensors were wired in parallel, then connected via a 1kΩ pull-up resistor to a 7.9V DC power supply. This provides sufficient current through each thermistor to drive it safely into self-heating mode. 1024 readings of the 'tap voltage' of the voltage divider were recorded at a 1Hz rate during a standard system time-constant measurement. Rate of water level rise was detectable as small step changes in the output voltage of the thermistor level sensing circuit as the arrival of the wetting front quenched each thermistor in turn (Figure 10).

This data set was used to compute the time the water took to rise past each of the ten level sensors; a line-of-best-fit for this water height versus time data set was determined using a variant of equation 12 of the form: -

$$h(t) = H - \exp\left(\frac{(t-offset)}{\tau} + \ln(H)\right) \qquad (17)$$

which returned a time-constant τ = 184 s (theoretically 174 s).

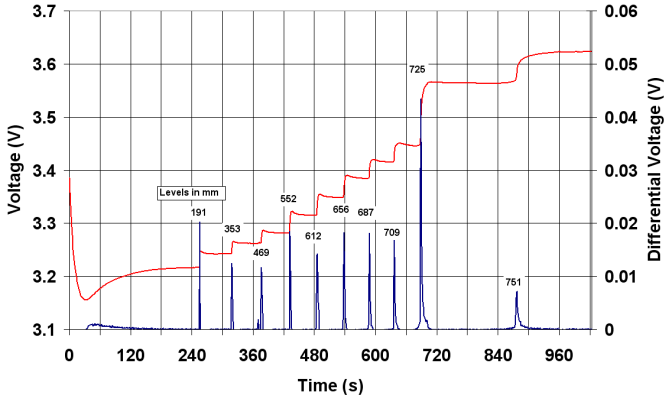

Figure 10. Temperature trace recorded from the ten-stage water level sensor array in the sensor standpipe. Water moves into the system from $t=0$, reaching heated NTC sensors at 191, 353, 469, 552, 612, 656, 687, 709, 725 and 751 mm at the times shown. Water height in the main tank was 793 mm. The voltage (left axis) is differentiated (right axis) to resolve the rate of water rise in the sensor standpipe.

The variable '*offset*' has the units of seconds and compensates for uncertainties in the actual start time for flow in the sensor standpipe, which depends upon the time taken to change the sensor height H in Figure 9.

The proportion of variance explained was r^2=99.94%.

Figure 11 shows the rise in water level and the fall in velocity within the sensor standpipe based upon Equation 17.

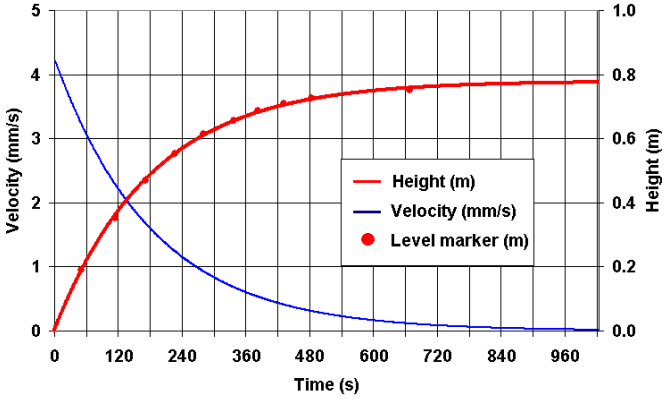

Figure 11. Height and velocity within the standpipe for a non-turbulent flow in the Hagen-Poiseuille control pipe of the 'single-sweep' calibration rig #2. Time $t=0$ was set to correspond to a point where the rising water column had covered the sensor by 50 mm.

E. *Flow results using the single-sweep calibration rig #2*

The measured system time constant τ from Eq. 17 of 184 s (as distinct from the predicted time constant of 174 s from Eq. 13) was used to transform experimental temperature-versus-time data to temperature-versus-velocity data. Standpipe vertical flow speed at every 1-second sample point was computed from the derivative of Eq. 12 as the rate of change in height (in mm): -

$$v_t(mm/s) = \frac{dh}{dt} = \frac{1}{\tau} e^{\left(\frac{-t}{\tau} + \ln H\right)} \qquad (18)$$

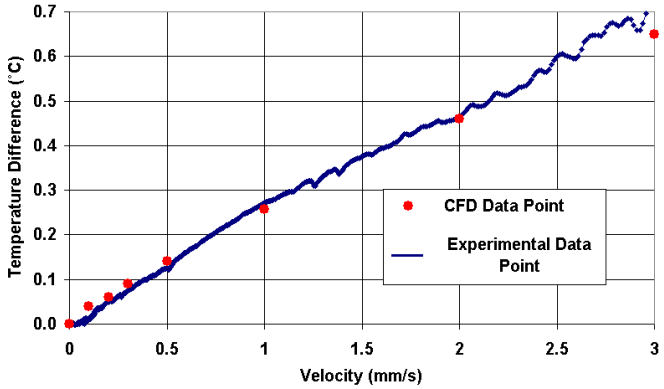

Figure 12. Sensor temperature difference T_S-T_F output (blue trace) versus velocity in mm/s for calibration rig #2. The large red data points are the predicted data points based upon the CFD model of a horizontal probe

The thermistor sensor was operated in self-heating mode throughout the calibration run. T_F was measured at a 1Hz rate to a precision of better than 0.001°C. Temperature data is only collected once the sensor tip is covered by water to a depth of 50 mm, and for standpipe velocities below 3 mm/s, as set by the inlet pipe length and bore diameter. The value for the still water temperature T_S was taken to be the water temperature at the end of the calibration run, when flow-

induced temperature changes fell to the level of background ambient temperature drift.

Temperature difference T_S-T_F from Calibration Rig #2 is plotted versus standpipe velocity (mm/s) in Figure 12.

The linear calibration equation for the single-sweep calibration method #2 is: -

$$v = 4.125(T_S - T_F) \quad (19)$$

with the proportion of variance explained r^2 = 99.46%

The slowest flow speed detectable using the single-sweep technique was 0.03 mm/s.

V. Discussion and Conclusions

The 'constant power' method of self-heating an NTC thermistor, developed by Skinner and Lambert (2008), has been used to measure the temperature of a flow-sensing thermistor while self-heating is occurring. Very slow flow measurements have been demonstrated for open-water bodies (Calibration Method #1) and large-bore vertical pipes (Calibration Method #2). In a working seepage meter standpipe the flow would need to be controlled by a valve arrangement to determine the still-water temperature T_S (valve shut: no flow) and T_F (valve open: flow established).

A theoretical model of a spherical thermal sensor made use of the Peclet number method; this agreed with the CFD model for flows between 3 mm/s and 100 mm/s. However this theoretical model was of no value below 3 mm/s when vertical buoyancy flows of up to 1.2 mm/s predicted by the CFD model interact with the background fluid flow.

Two experimental set-ups have been used to demonstrate the warm thermistor flow meter's response below 3 mm/s and as low as 0.03 mm/s. The plunging probe method is the more precise of the two, but is more labour-intensive than the standpipe method. Using the vertical standpipe calibration system, a good correlation was found between the theoretical time constant (τ=174 s) based upon physical parameters and dimensions, and that achieved in practice using multiple level sensors (τ=184 s).

A simple linear gain relationship has been found between the temperature difference T_S-T_F and the flow velocity v with two different experimental set-ups and a CFD model for flow velocities below 3 mm/s. Linear gain coefficients for both sets of calibration apparatus gave similar gain coefficients of 4.44 and 4.125 respectively (Eqs. 6 and 19), compared to 4.45 for the CFD model (Eq. 7). A single point linear calibration should therefore be acceptable.

Other authors (e.g Yu et al 1993) have found a similar linear relationship in MEMS sensors at very slow flow rates to that found here using a spherical warm-thermistor flow sensor. At velocities below 3 mm/s, buoyancy becomes a dominant mechanism affecting heat transfer, modifying the velocity field local to the probe. As bulk fluid velocity reduces, the Grashof number increases due to the increasing temperature differential. This increases the convective heat transfer (Nusselt number) which suppresses the temperature rise of the thermistor. A balance is achieved whereby the heat input equals the heat dissipation at an equilibrium temperature that is dependent on the bulk fluid velocity. This linearity disappears in the CFD model if the buoyancy is switched off (Grashof number approaches zero).

The effect of bio-film build-up under field conditions is a potential source of long-term drift in the sensor as suggested by Equation 4 and Figure 2. No attempt has been made experimentally to quantify this drift in the sub-3 mm/s flow range where Equation 4 itself proved to be invalid; such an assessment is best made under field conditions with and without biofilm suppression.

A computational fluid dynamics model was used to predict the sensor's response over the wider flow range between 3 mm/s and 100 mm/s, although no attempt has been made in the current paper to describe a calibration method for this flow range. The CFD response over this extended flow range does suggest, however, that the sensor should operate successfully up to temperature differentials of 2ºC or more. Tests of the thermistor's response in a strong water jet of hundreds of mm/s gave a temperature differential of 3ºC, suggesting that the same sensor control circuit would function adequately – albeit with lower flow resolution – at flow rates above 100 mm/s. The sensor turn-down ratio is therefore better than 1000:1, which is important in seepage meters, as numerous studies have shown that seepage fluxes vary over three to five orders of magnitude.

These laboratory results suggest that a simpler version of the seepage meters of Taniguchi and Paulsen could be manufactured with this sensor technology, using a single thermistor sensor mounted directly in the vertical throat of the seepage meter rather than as a horizontal attachment as used by both these authors. If this sensor were placed in the throat of a seepage meter having the same bell-to-throat ratio of 2964:1 as Paulsen's meter, then the instrument would be capable of resolving groundwater flows as low as 10 nm/s, or 0.9 mm/day at a throat velocity of 0.03 mm/s.

ACKNOWLEDGMENT

The authors thank Dr. Allan Wallace of Avocet Consulting in Adelaide South Australia for his assistance with the CFD (Phoenics) modelling of the probe velocity and heat fields, Mr Jack Hoogland of Measurement Engineering Australia for help with the Hagen-Poiseuille method, and Dr. Paul Hutchinson of CSIRO Land and Water (Griffith NSW Australia) for his help with the Peclet Number model.

REFERENCES

[1] Brand, A.,Müller, B., Wuest, A., Dinkel, C., Revsbech, N. P., Nielsen, L.P., Pederesen, O., Damgaard, L. R., Larsen, L. H. and Wehrli, B. (2007). 'Microsensor for in situ flow measurements in benthic boundary layers at submillimeter resolution with extremely slow flow.' Limnology and Oceanography: Methods 5, 185-191

[2] Clift, R., Grace, J. and Weber, M. E., 'Bubbles, Drops and Particles' (1978). Dover Publications. ISBN: 9780486445809

[3] Lee, D.R. (1977). 'A Device for Measuring Seepage Flux in Lakes and Estuaries' *Limnology and Oceanography*, Vol. 22, No. 1 (Jan., 1977), pp. 140-147

[4] MacIntyre, S., (1986). 'A flow-measuring system for use in small lakes.' Limnology and Oceanography, 31(4), 900-906.

[5] Paulsen, R.J., Smith, C.F., O'Rourke, D., Wong, T.F. (2001) 'Development and evaluation of an ultrasonic ground water seepage meter' - Ground Water, Vol.39, No. 6, p 904-911, Nov/Dec 2001

[6] Riedl, R. J., Machan, R. (1972). 'Hydrodynamic patterns in lotic intertidal sands and their bioclimatological implications.' Marine Biology, 13, 179-209.

[7] Rosenberry, D.O., Morin, R.H. (2004) 'Use of an electromagnetic seepage meter to investigate temporal variability in lake seepage'. Ground Water, Vol 41(1). p 68-77. Jan/Feb 2004

[8] Roy, H., M. Hüttel, and B B. Jørgensen 2002. The role of small-scale sediment topography for oxygen flux across the diffusive boundary layer. Limnol. Oceanogr. 47: 837-847.

[9] Skinner, A.J. Lambert, M.F. (2008). 'Continuous measurement of plant water status using a constant-power warm thermistor sensor'. Submitted to IEEE Sensors Journal, March 2008.

[10] Spitzer, D. W. 'Industrial Flow Measurement', 3rd Edition 2005, ISA. ISBN 978-1-55617-871-9

[11] Steinhart, J.S. Hart, S.R. 'Calibration Curves for Thermistors'. Deep Sea Research Vol. 15 p. 497 (1968)

[12] Taniguchi, M., Fukuo, Y. (1993) 'Continuous Measurements of Ground-Water Seepage Using an Automatic Seepage Meter'. Ground Water GRWAAP, Vol. 31, No. 4, p 675-679, July/August 1993.

[13] Yu, D., Hsieh, H.Y. and Zemel (1993) 'Microchannel pyroelectric anemometer'. Sensors and Actuators A, 39 (1993) 29-35

Andrew J. Skinner FIEAust obtained a Bachelor of Technology degree in Electronic Engineering in 1975 and a Master of Electronic Engineering in 1987 at the South Australian Institute of Technology.
Andrew worked in Australia, Papua New Guinea and Canada as a nucleonic instrumentation design engineer in the mineral processing industry. He returned to Australia in late 1982 to specialise in data logging applications and environmental measurement systems, founding Measurement Engineering Australia in 1984. He is currently the engineering director at MEA.

Martin F. Lambert FIEAust is currently an Associate Professor in the school of Civil and Environmental Engineering. He joined the University of Adelaide in 1995 after completing his PhD at the University of Newcastle, Australia. He research areas include river hydraulics, pipeline condition assessment and stochastic hydrology.